


Minocycline-Loaded Titanium Dioxide Nanoparticles for Augmented Synergistic Periodontal Sonodynamic Chemotherapy

Shuying Huang^{1,2,*}, Chengyao Xia^{3,*}, Wenbao Zuo³, Rui Wang², Nuo Xu², Wenxin Ye², Xiao Li², Yong Chen² , Xuan Zhu³

¹Xiamen University School of Public Health, Xiamen, People's Republic of China; ²Department of Stomatology, School of Medicine, Xiamen University, Xiamen, People's Republic of China; ³Fujian Provincial Key Laboratory of Innovative Drug Target Research, School of Pharmaceutical Sciences, Xiamen University, Xiamen, 361102, People's Republic of China

*These authors contributed equally to this work

Correspondence: Yong Chen; Xuan Zhu, Email yongchen@xmu.edu.cn; zhuxuan@xmu.edu.cn

Background: The current clinical treatment of periodontitis usually involves mechanical removal of pathogenic bacteria through ultrasonic scaling and root planing, supplemented with antibacterial medications to inhibit microbial overgrowth. However, the therapeutic efficiency remains unsatisfactory due to complicated periodontal anatomy, limited plaque removal, short retention of antibiotics, and related side effects.

Methods and Results: To address these issues, we successfully synthesized mesoporous titanium dioxide nanoparticles (MTN) via a sol-gel method, which were modified with hemoglobin (Hb) and loaded with minocycline (MINO). The resulting Hb-MTN/MINO nanoparticles had a size of 215 nm, zeta potential of $-19.8 \text{ mV} \pm 0.9 \text{ mV}$, and uniform shape with a PDI index of 0.176. The modification with hemoglobin (Hb) provided sufficient oxygen for antimicrobial sonodynamic therapy (aSDT), contributing to improved generation of reactive oxygen species (ROS) under low ultrasound intensity. After MINO loading, the system exhibited notable antibacterial efficacy, with a 6 log reduction of bacterial counts compared to the control group. Hb-MTN/MINO was evaluated in vivo in terms of oral index, soft and hard tissues, along with biosafety evaluation in periodontal disease model rats. Hb-MTN/MINO demonstrated a satisfactory therapeutic effect, whereby the periodontal condition of the rats exhibited a greater improvement than the control group, and measurement of the serum levels of inflammatory factors revealed that both IL-6 and MMP-9 were significantly downregulated.

Conclusion: These findings confirm the potential of Hb-MTN/MINO nanoparticles as a promising treatment option for periodontitis.

Keywords: periodontitis, nanoparticles, sol-gel method, sonodynamic therapy, minocycline

Introduction

Periodontitis is a destructive chronic inflammatory disease that is initially caused by colonization of periodontal pathogens and an imbalance between microorganisms and host defenses.¹ Notably, evidence from epidemiological studies indicates that periodontal disease is associated with an increased risk of systemic diseases, such as cancer, atherosclerosis, diabetes, chronic bronchitis and rheumatoid arthritis.^{2–6} Moreover, there is an emerging global epidemic of periodontitis with increasing prevalence, mainly attributed to its complicated etiology and challenging treatment, making it the most common oral disease worldwide.⁷ It affects millions of people each year and has evolved into a major public health issue.^{8,9} It has been reported that 42% of adults in the United States suffer from periodontitis and nearly 7.8% have severe periodontal problems.¹⁰ As periodontitis progresses, it can also cause damage to the soft and hard tissues that support the teeth, resulting in the destruction of the gum and periodontal ligaments, progressing to the

absorption of the alveolar bone.¹¹ Finally, in its most severe form, periodontal disease can lead to tooth loss and severely decrease the quality of daily life.^{12,13}

The etiology of periodontitis is multifaceted, but the culprit remains bacterial colonization of periodontal tissues.^{7,14} Hence, major treatment strategies generally focus on suppressing bacteria and counteracting their detrimental effects. In clinical practice, fundamental therapy is primarily based on mechanical surface debridement to remove microbial plaques by scraping the infected dental bed in a nonsurgical manner.^{15–17} It can offer satisfactory control of periodontitis for a short period, but pathogens in soft tissue and other anatomically inaccessible areas (eg, furcation and root depressions) are not accessible, so that they inevitably re-invade periodontal tissues.¹⁸ Although periodontal surgery is another alternative, it is unacceptable for most patients owing to the associated pain and high cost. Currently, chemotherapy is combined with mechanical treatment to improve therapeutic outcomes.^{17–19} However, it should be noted that with the widespread use of antimicrobials, a wide variety of problems have emerged, including multidrug resistance of bacterial pathogens, side effects associated with antibiotics, and challenging systemic management.²⁰

Antimicrobial photodynamic therapy (aPDT) is a novel approach that utilizes specific wavelengths of light to stimulate photosensitizers to produce highly toxic reactive oxygen species (ROS), which kill pathogenic microorganisms by oxidatively damaging biomolecules (eg, phospholipids, enzymes, proteins, and DNA), and has been widely used to fight bacterial infections. However, it has inherent deficits, such as low tissue penetration depth and severe phototoxicity after systemic use of photosensitizers. In recent years, researchers developed antimicrobial sonodynamic therapy (aSDT) as a new non-invasive treatment modality derived from aPDT, in which microorganisms are killed by the combination of low-intensity ultrasound and acoustic sensitizers to generate ROS, overcoming the problem of the limited depth of light penetration in aPDT. In addition to ROS production, aSDT also promotes mechanical debridement through cavitation. The synergistic combination of ROS and mechanical cavitation in aSDT not only reduces the membrane potential, but also visibly damages the cell membrane structure.^{21,22} Notably, the high safety, deep penetration, and low cost of aSDT make it a promising antimicrobial therapeutic approach for dentistry.²³

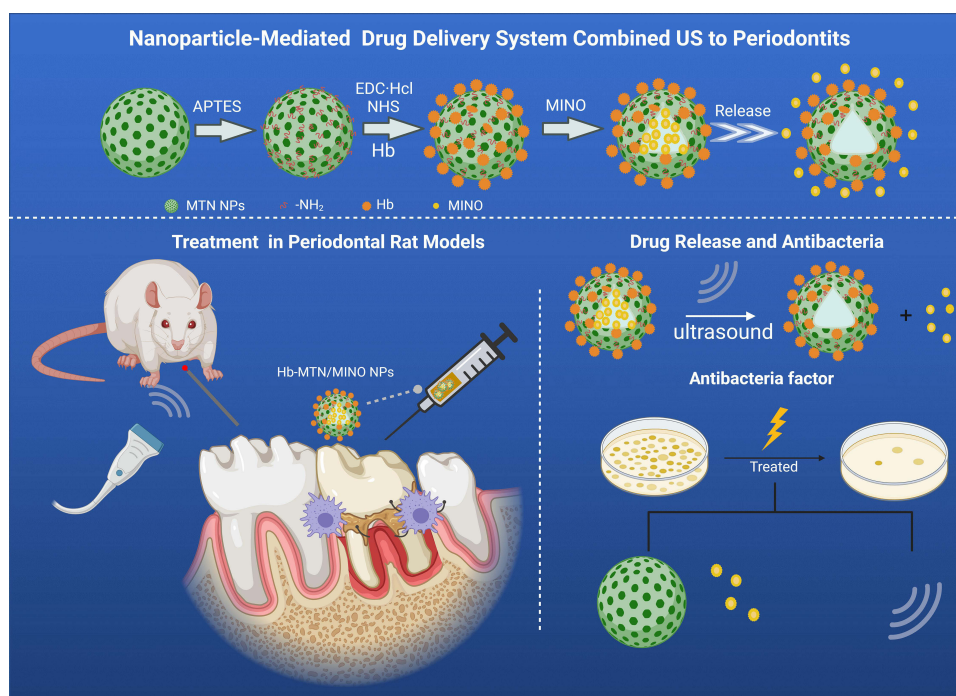
However, the inherent hydrophobicity of typical acoustic sensitizers, resulting in their poor dispersion and low water solubility under physiological conditions, leads to low ROS production, which currently limits their efficacy. The rapid development of nanoparticles for drug delivery has enabled continued innovation in medicine in recent years. Metal oxide nanoparticles MONPs have a wide range of applications in the industrial and biomedical fields due to their antibacterial, antifungal, and photocatalytic activities, as well as biosafety and biocompatibility. Inorganic nanoparticles such as titanium dioxide (TiO₂) and barium titanate (BTO) can be directly used due to their inherent acoustic sensitizer properties.¹⁹ In addition, the nanostructures of these inorganic acoustic sensitizers not only provide more nucleation sites for ROS generation, but also show better stability in SDT applications.

Here, we developed a drug carrier platform primarily based on mesoporous titanium dioxide nanoparticles (MTN), an inorganic sonosensitizer with good biocompatibility and high stability.^{24–26} After loading with the antibiotic minocycline (MINO), the device exhibited enhanced antimicrobial properties.^{2,3} Moreover, encapsulation in nanoparticles attenuated the drug toxicity of MINO, effectively reducing the damage to periodontal cells. Notably, the process of ROS generation by sonosensitizers during SDT requires the participation of O₂.²⁷ It is worth noting that in the case of periodontal disease, less than 2% of atmospheric oxygen is available in periodontal pockets, which greatly impacts the antibacterial effect of SDT.²⁸ To tackle the hypoxic conditions of the periodontium, hemoglobin (Hb) was conjugated onto the surface of nanoparticles through an acylation reaction, thereby providing additional oxygen to improve the utilization efficiency of ultrasonic energy during SDT. Based on this approach, the Hb-MTN/MINO NPs drug delivery system was developed to achieve a combined antibacterial effect via the generated ROS and loaded MINO, as shown in [Scheme 1](#).

Materials and Methods

Materials, Cell Lines, and Animals

Titanium (IV) isopropoxide (TTIP, 97%), Pluronic (F68), hemoglobin from bovine blood (Hb 98%), 2-morpholinoethanesulfonic acid monohydrate (MES, 99%), minocycline hydrochloride (MINO, 99%), tris(4,7-diphenyl-1,10-phenanthroline) ruthenium(II) dichloride ([Ru(dpp)₃]Cl₂, 95%), 9,10-anthracenediylbis(methylene)dimalonic acid



Scheme 1 Schematic illustration of the preparation procedure of Hb-MTN/MINO NPs (top) and the proposed antibacterial mechanism of the synergistic modality of sonodynamic-chemotherapy (bottom). Created in BioRender. Xia, C. (2025) <https://BioRender.com/b96b004>.

(ABDA, 98%), 3-(4,5-dimethyl-2-thiazolyl)-2,5-diphenyltetrazolium bromide (MTT, 98%) were purchased from Sigma-Aldrich LLC (Beijing, China). The calcein-AM/PI double staining kit was purchased from KeyGEN Biotech Co. Ltd (Nanjing, China). Dulbecco's modified Eagle's medium (DMEM), fetal bovine serum (FBS), PBS, penicillin-streptomycin antibiotic mixture, and trypsin-EDTA (no phenol red, 0.5% trypsin) were acquired from HyClone (USA). Blood biochemical index detection kits (ALT, AST, TP, AKP, BUN, ALB, and CRE) were obtained from Nanjing Jiancheng Co. Ltd (China). The enzyme-linked immunosorbent assay (ELISA) kit was purchased from Guangzhou Caozhiyuan Co. Ltd.

Human gingival Fibro cells (HGF-1, MeisenCTCC) and mouse fibroblasts (L929, ProcellNCTC) were cultured in DEME medium containing 10% FBS and 1% penicillin-streptomycin in a humidified incubator with 5% CO₂ at 37 °C. *Porphyromonas gingivalis* (ATCC BAA-308), *Aggregatibacter actinomycetemcomitans* (ATCC29523), and *Fusobacterium nucleatum* (ATCC25586), were obtained from Guangdong Microbial Culture Collection Center (GDMCC). *P. gingivalis* and *F. nucleatum* were cultivated on blood agar plates (HKM HuanKai Microbial, China) at 37°C under anaerobic conditions (85% N₂, 10% H₂ and 5% CO₂), while *A. actinomycetemcomitans* was incubated aerobically (95% air, 5% CO₂). All experimental animals were supplied by the Xiamen University Laboratory Animal Center and experiments were carried out according to protocols approved by the Institutional Animal Care and Use Committee of Xiamen University. All in vivo experiments were carried out according to the approved guidelines (Approval No.: XMULAC20190001).

Establishment of the MINO Standard Curve

A sample comprising 10.00 mg of MINO was weighed precisely using an analytical balance, and 5 mL of the master mix (concentration 2 mg/mL) was prepared in PBS (pH 7.4). This solution was then diluted with PBS (pH 7.4) to 200 µg/mL, 100 µg/mL, 50 µg/mL, 25 µg/mL, and 12.5 µg/mL, after which 200 µL of each concentration of MINO was added into a 96-well transparent enzymological plate. Six replicate wells were set up for each concentration, and the absorbance values at 375 nm were recorded using a microplate reader. The standard curve of MINO was plotted according to the obtained data.

Synthesis of Hb-MTN/MINO NPs

Mesoporous titanium dioxide nanoparticles (MTN) were successfully fabricated using a conventional sol-gel method utilizing TTIP as a titanium resource and F68 as a template for structure orientation. Briefly, 0.8 g F68 was fully dissolved in 20 mL of ethanol, and 120 μ L of water was added. The mixture was vigorously stirred and 370 μ L of TTIP was slowly added. After becoming milky-white, the suspension was stirred for an hour, and left at room temperature overnight. After centrifugation, the obtained precipitate was dissolved in ethanol and stirred at 70 °C for two hours to release the template of F68. The MTN was then washed with ethanol and dried slowly to remove the solvent.

To prepare NH₂-MTN, 50 mg of MTN was dissolved in 20 mL of ethanol, after which 3-mercaptopropyl trimethoxysilane (APTES, 400 μ L) and ammonia (1 mL) were mixed together in this suspension. The resulting solution was stirred under N₂ for 12h. Finally, to obtain purified NH₂-MTN, the prepared samples were washed three times with ethanol and three times with water.

For further modification, Hb (10 mg) was completely dissolved in MES (50 mm, 5 mL, pH6.5) by sonication, activated by the addition of EDC·HCl (10 mg) and NHS (7.5 mg), and incubated for 30 min in the dark. NH₂-MTN (5 mg) was dissolved in an equal quantity of MES (50 mm, pH6.5) and then mixed with the above-mentioned solutions under stirring for another 12h. The unreacted reagents were washed off, and the resulting Hb-MTN particles were collected by centrifugation.

Different ratios of MINO/Hb-MTN were tested to achieve optimal loading. Briefly, 0.1 mg of the particles in aqueous solution was used in this experiment with different quantities of MINO (0.1 mg; 0.2 mg; 0.3 mg; 0.4 mg and 0.5 mg respectively). The suspension was stirred at 37°C for 8 h, and the supernatant was collected for spectrophotometric quantification at 375 nm. Finally, the loaded MINO amount was calculated as follows: $M_{loaded-MINO} = M_{prep-MINO} - M_{free-MINO}$. The corresponding loading capacity was calculated using the formula:

$$Drug\ loading\ capacity = \frac{M_{loaded-MINO}}{M_{Hb-MTN} + M_{loaded-MINO}} \times 100\%$$

Characterization of Hb-MTN/MINO NPs

The morphology of the nanoparticles was observed by transmission electron microscopy (TEM; JEM-1230, Tokyo, Japan). Dynamic light scattering (DLS; Zetasizer Nano ZS-90, Malvern, UK) was used to estimate the sample distribution and zeta potential. Ultraviolet-visible (UV-vis) and FT-IR spectra were recorded to monitor the changes of content, and energy-dispersive X-ray spectroscopy (EDS) was employed to analyze the chemical composition of the Hb-MTN/MINO NPs.

Evaluation of Oxygen Generation and US Sensitivity

To assess the effects of Hb modification, an oxygen sensor was used to evaluate the oxygen release kinetics of free and modified Hb. Briefly, [Ru(dpp)₃]Cl₂ (50 μ g) was added to the Hb solution (0.5 g/L) and Hb-MTN/MINO suspension (Hb equivalent), after which the intensity was monitored at the predetermined time (I_n) by fluorescence microscopy measurements (λ_{ex} = 455 nm; λ_{em} = 610 nm). The fluorescence intensity of Ru(DPP)₃Cl₂ was recorded as I_0 , and the total oxygen generation was expressed as $\ln(I_n/I_0)$.

The singlet oxygen fluorescence probe ABDA was used to evaluate the ROS generation triggered by ultrasonication. To verify the SDT potential, Hb-MTN/MINO NPs (1.5 mL of various concentrations) were mixed with ABDA (100 ng/mL, 50 μ L) and then subjected to ultrasonication (power intensity: 1 W/cm², frequency: 1 MHz). The samples were analyzed by fluorescence spectroscopy (λ_{ex} = 360 nm, λ_{em} = 610 nm).

Investigation of pH-Responsive Drug Release

To investigate drug release kinetics, Hb-MTN/MINO solutions (5 mL) were dialyzed using a semi-permeable membrane (10 kDa molecular weight cutoff) in 50 mL of PBS equivalent at different pH values (pH= 5.6, 6.4, and 7.4). The system was kept at 37°C with gentle stirring. Aliquots comprising 1 mL were collected at the indicated intervals for spectrophotometric quantification, and an equivalent volume of fresh PBS was added to the system.

Cytotoxicity Assay

The cytotoxicity of the Hb-MTN/MINO NPs was detected using HGF-1 and L929 cells. To evaluate cell viability over time, HGF-1 cells were seeded into 96-well plates at a density of 6×10^3 cells per well and treated with Hb-MTN/MINO NPs (0, 10, 20, 40, and 80 $\mu\text{g/mL}$) for different intervals (6, 12, 24, and 48 h), after which viability was assessed using the standard MTT assay. Additionally, to determine the cytotoxicity of MINO, L929 cells were treated with free MINO and Hb-MTN/MINO NPs (MINO equivalent) and cell viability was measured 48 h later. L929 cells that underwent the same treatment were stained using a Calcein-AM/PI double staining kit to quantify live and dead cells by fluorescence microscopy ($\lambda_{\text{ex}} = 488 \text{ nm}$, $\lambda_{\text{em}} = 530 \text{ nm}$).

Antibacterial Effects in vitro

Three representative gingival bacterial species (*P. gingivalis*, *F. nucleatum*, *A. actinomycetemcomitans*) were selected to evaluate the antibacterial properties of Hb-MTN/MINO NPs. The cryopreserved bacteria were resuscitated on blood agar plates and transferred to brain heart infusion (BHI). First, the growth curve and minimal inhibition concentration were evaluated by measuring the optical density at 600 nm (OD_{600}). Before evaluating antibacterial activity, the cultured bacteria were collected and adjusted to a working concentration of 10^6 CFU mL^{-1} for further experiments. The following six groups were included.

- (1) PBS without ultrasonication (control).
- (2) PBS with ultrasonication (control + US).
- (3) Hb-MTN without ultrasonication (Hb-MTN).
- (4) Hb-MTN with ultrasonication (Hb-MTN + US).
- (5) Hb-MTN/MINO without ultrasonication (Hb-MTN/MINO).
- (6) Hb-MTN/MINO with ultrasonication (Hb-MTN/MINO + US).

Bacteria ($10 \mu\text{L}$, 10^6 CFU mL^{-1}) were plated into 24-well plates containing $900 \mu\text{L}$ BHI broth and then treated with PBS, Hb-MTN NPs, or Hb-MTN/MINO NPs ($100 \mu\text{L}$, MIC concentration), followed by ultrasonication (power intensity: 1 W/cm^2 , frequency: 1 MHz). After 48 h of treatment, the bacteria were spread on blood agar plates to count the colony-forming units. To verify the metabolic ability, bacteria were subjected to the same treatment as described above, and evaluated by the MTT assay. SEM images were used to demonstrate the morphological changes in the bacteria under various treatments.

In vivo Therapy Efficacy of Hb-MTN/MINO NPs Combined With SDT for Periodontal Inflammation in Model Rats

Female Wistar rats (3–6 months, $180 \pm 20 \text{ g}$) were supplied by the Xiamen University Laboratory Animal Center, and the experiment complied with all relevant ethical regulations for animal testing. Experimental rat models were established using a previously established method with multifactorial interventions. First, a 4–0 sterile silk thread was placed around the cervical margins of the second molar, followed by a continuous 7-day injection of *P. gingivalis* suspension (10^6 CFU/mL , $100 \mu\text{L}$). At the same time, 10% sugar syrup and normal chow diet were fed to accelerate the development of inflammation. After modeling, the rats were randomly divided and a control group consisting of healthy rats was included. These mock-treated animals received an injection of PBS to control for the stimulating effects caused by the local injection. Consequently, local treatment was performed with subgingival injection ($100 \mu\text{L}$) every other day 4 times, and the therapeutic efficacy was evaluated. The seven groups ($n=3$) were treated as follows.

- (1) Model rats of periodontal disease without any treatment (PD);
- (2) Healthy rats with PBS injection (Normal);
- (3) Model rats of periodontal disease treated with PROCLINE[®] (PROCLINE);
- (4) Model rats with periodontal disease with Hb-MTN NPs injection (Hb-MTN)

- (5) Model rats with periodontal disease with Hb-MTN NPs injection and ultrasonication (Hb-MTN+US)
- (6) Model rats with periodontal disease with Hb-MTN/MINO NPs injection (Hb-MTN/MINO)
- (7) Model rats with periodontal disease treated with Hb-MTN/MINO NPs injection and ultrasonication (Hb-MTN/MINO+US).

The body weight of the rats was recorded during treatment, while the gingival index (GI) and gingival sulcus bleeding index (SBI) were used to assess their oral health. Before euthanasia, blood was collected from the main thigh artery to determine biochemical indices (ALT, AST, TP, AKP, BUN, ALB, and CRE), and quantify inflammatory factors (IL-1 β , IL-6, TNF- α , and MMP-9) in the serum using ELISA. Moreover, The upper jaw of rats with teeth and periodontium was removed and washed with physiological saline, after which it was fixed with paraformaldehyde (4%). This sample was scanned with a micro-CT scanner to evaluate periodontal bone tissues, which were reconstructed using CT Vol software (Skyscan, Bruker-micro CT) to measure the distance between the cemento-enamel junction (CEJ) and alveolar bone crest (ABC). Jaws were collected for histological analysis of the second molar. H&E staining was performed on the main organs (heart, liver, spleen, lungs, and kidneys), followed by analysis using an imaging system BX53M (Olympus, Japan).

Statistical Analysis

Quantitative data were expressed as means \pm standard deviations (SD, $n \geq 3$). Data were analyzed using GraphPad Prism version 8.0.2 (GraphPad Software Inc., San Diego, CA, USA), and statistical significance was assessed using single-factor analysis of variance (one-way ANOVA) with Duncan's multiple range test for comparison of multiple groups, while Student's *t*-test was used for two-group comparisons (SPSS software, version 20.0, SPSS Inc.). The indicated *p*-values ($*p < 0.05$, $**p < 0.01$) and lowercase letters denote significant differences. Means within columns followed by different letters are significantly different.

Results and Discussion

Characterization of Hb-MTN/MINO NPs

MTN NPs were successfully synthesized via a previously published sol-gel method using TTIP as the raw material. As shown in [Figure 1A](#), the transmission electron microscopy (TEM) images demonstrated that the MTN NPs were spherical and monodisperse, with an average diameter of approx. 200 nm and a clear mesoporous structure. In this study, the MTN NPs were designed as a drug delivery platform. The MTN was functionalized with APTES and then subjected to an amide reaction via activation with EDC·HCl and NHS. As a result, Hb was conjugated the MTN surface. Nitrogen adsorption-desorption isotherms confirmed that the Bruno-Em-Taylor (BET) surface and pore sizes were 157 m²/g and 11.7 nm, respectively. Then, the Hb-MTNs were loaded with MINO under mild stirring at 37°C. A series of characterization experiments were performed to evaluate the successful preparation and relevant properties. Dynamic light scattering (DLS) was used to record the zeta potential during the process, and more positive charges were introduced on the surface of the nanoparticles via amination, which was later neutralized by carboxyl groups from Hb ([Figure 1B](#)).

The final synthesized Hb-MTN/MINO was estimated to have a zeta potential of $-19.8 \text{ mV} \pm 0.9 \text{ mV}$, and particle size of 215 nm, with a PDI of 0.176. This indicated the homogeneous morphology and good dispersibility of Hb-MTN/MINO ([Figure 1C](#)). According to the TEM results, there was only a slight increase in size due to modification and drug loading, while there was hardly any change in morphology. Moreover, elemental distribution mapping of Hb-MTN/MINO was performed using high-resolution TEM combined with energy-dispersive spectroscopy (EDS). As depicted in [Figure 1D](#), S was uniformly distributed on the surface of the nanoparticles, confirming the success of Hb conjugation. As expected, Ti, O, C, and N were also present. The UV-vis spectra showed that MTN had a strong absorption peak at 250–282 nm, which did not change significantly after the amination reaction. An absorption peak of Hb-MTN was observed at 405 nm, confirming its successful conjugation. A similar characteristic absorption peak was observed in the final preparation of Hb-MTN/MINO. However, Hb-MTN/MINO did not exhibit relevant MINO absorption peaks at 290 nm and 375 nm.

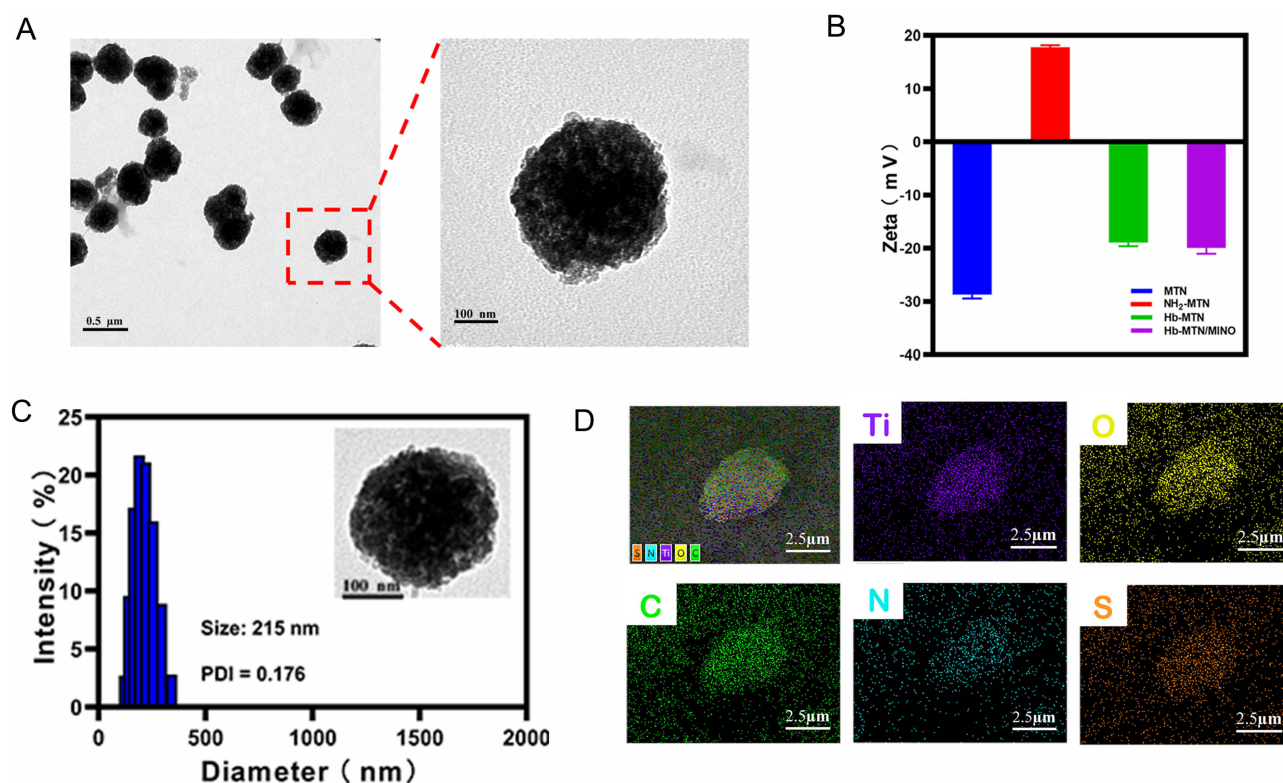


Figure 1 (A) TEM images of synthesized MTN NPs; (B) Zeta-potentials of MTN, NH₂-MTN, Hb-MTN, and Hb-MTN/MINO. (C) Size distribution of Hb-MTN/MINO and TEM image. (D) EDS elemental mapping images Hb-MTN/MINO NPs.

This is probably because the strong absorption from the MTN overlaps with and thereby covers this wavelength range (Figure 2A). Additionally, the FT-IR spectra provided direct evidence, including peaks attributed to amino groups (1015 cm^{-1}) and amide bonds (1688 cm^{-1}), as well as benzene rings (3000 cm^{-1} and 1498 cm^{-1}) validating successful drug loading (Figure 2B). Different ratios of MINO to Hb-MTN were investigated to define the appropriate dosing ratios and the corresponding drug-loading efficiencies. As the ratio increased, the drug-loading efficiency improved significantly but then stabilized (Figure 2C). It therefore stands to reason that the capacity of the mesoporous structure was close to saturation at a ratio of 2:1. To ensure the full utilization of MINO, a MINO: Hb-MTN ratio of 2:1 was selected, which resulted in a drug loading efficiency of 17.3%. The final formulation (Hb-MTN/MINO) was assessed at different pH values (5.6, 6.4, 7.4) and dialyzed in equivalent PBS at 37°C . The release behavior is shown in Figure 2D. Sustained release mostly occurred in the first 48 h. Afterwards, even though Hb-MTN/MINO was still continuously released, the rate was much lower. Significantly, almost 78.8% of the drug was released within 48 h at pH 6.4, which was 13.7% higher than at pH 5.6, and 38.5% higher than at pH 7.4. Therefore, it is reasonable to conclude that drug release is more favorable in an acidic environment, which is consistent with the microenvironment of periodontitis. Sucrose fermentation by periodontal microorganisms leads to a rapid decrease of the pH in the biofilm matrix, resulting in a consistently low-pH environment.²⁹ This acidic environment disrupts microbial homeostasis in the dental ecological niche and promotes the growth of acid-tolerant organisms.^{30,31} However, the hypoxic microenvironment of the periodontal pockets poses an additional challenge. ROS are formed through oxidation reactions or electronic excitation and mainly include hydroxyl radicals ($\cdot\text{OH}$), superoxide anions ($\cdot\text{O}_2$), and singlet oxygen ($^1\text{O}_2$), which are derived from O_2 .³² Accordingly, Hb was conjugated onto the surface of the nanoparticles so that there is sufficient oxygen in periodontal tissues, contributing to ROS generation. Ru[dpp]₃Cl₂, an oxygen indicator with yellow fluorescence, was used to quantify the oxygen-release behavior of free Hb and Hb-MTN/MINO (containing equal amounts of Hb). As shown in Figure 2E, the oxygen content gradually increased with time and then tended to reach saturation, indicating that oxygen was completely released. In contrast to Hb alone, oxygen release from Hb-MTN/MINO was significantly higher because free Hb was unstable and

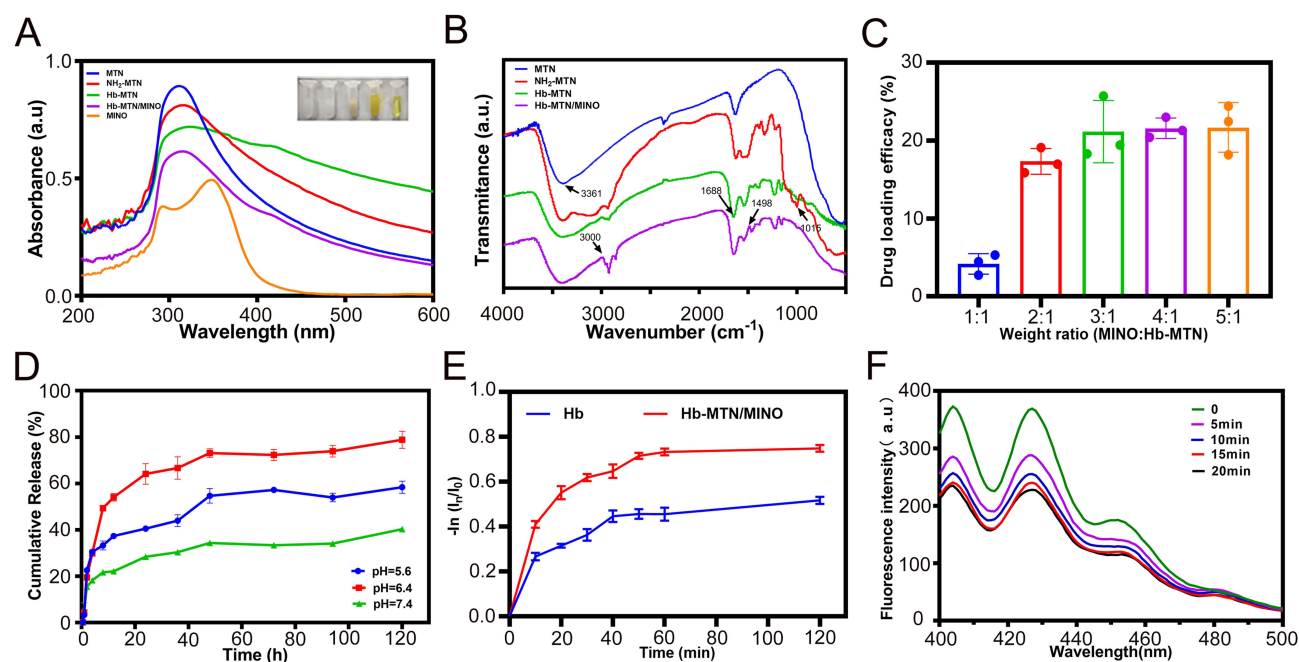


Figure 2 (A) FT-IR spectra of MTN, NH₂-MTN, Hb-MTN, and Hb-MTN/MINO. (B) UV-visible spectra of MTN, NH₂-MTN, Hb-MTN, Hb-MTN/MINO, and MINO. (C) Drug loading efficacy at different weight ratios of MINO to Hb-MTN. (D) Drug release behavior of Hb-MTN/MINO at different pH values in vitro; (E) Oxygen release in vitro. (F) Fluorescence spectra of ABDA after co-incubation with the same concentrations of Hb-MTN/MINO sonicated for different time intervals.

only a small amount of oxygen was released, while the stability was enhanced when Hb was attached to the surface of nanoparticles. Thus, Hb-MTN/MINO promoted oxygen release, which enhanced the effect of SDT. It therefore reasonable to conclude that the hypoxic environment could be relieved to some degree by Hb modification, so that the Hb-MTN/MINO NPs system may promote a more conducive periodontal microenvironment for the healing of inflammation. Furthermore, considering the sonodynamic activity of titanium dioxide, the drug delivery system can be activated by low-frequency ultrasound, resulting in enhanced ROS generation. When the level of ROS exceeds a certain threshold, they can react with various biomolecules and induce protein denaturation, leading to oxidative degradation of lipids and damage to DNA, thus eliciting bacterial cell death.³³ Based on these results, the prepared Hb-MTN/MINO was designed to interact with oxygen under ultrasonication, and a specific fluorescent probe (ABDA) was used for evaluation. The solution of ABDA and Hb-MTN/MINO was activated by ultrasonic stimulation (power intensity: 1 W/cm², frequency: 1 MHz), resulting in a change of fluorescence intensity. As shown in Figure 2F, there was an obvious decrease in the fluorescence intensity with increasing sonication time, indicating an increase of ROS generation. However, when stimulated for 15 min or more, the fluorescence intensity reached a plateau. Thus, 15 min was selected as an appropriate sonication time for further experiments. In general, there was time-dependent SDT in Hb-MTN/MINO within a certain time range. Moreover, the ROS yield was concentration-dependent as well, as shown in Figure S1. These results confirmed ROS generation under ultrasonic stimulation using Hb-MTN/MINO NPs as a sonosensitizer. In summary, these findings indicated the successful construction of minocycline-loaded titanium dioxide nanoparticles.

Biosafety Evaluation in vitro

Human gingival fibroblasts (HGF-1) and mouse fibroblasts (L929) were employed to compare the cytotoxicity of free MINO and Hb-MTN/MINO (containing equivalent amounts considering the potential toxicity and biocompatibility of the drug-carrier nanoplatform) in vitro using the MTT assay. First, the cytotoxicity of Hb-MTN/MINO was investigated in HGF-1 cells. Viability decreased when the cells were exposed to Hb-MTN/MINO, but there was no distinct tendency for survival over time (Figure S2). Moreover, the total survival rate remained above 80%, indicating good biocompatibility of Hb-MTN/MINO. As shown in Figure 3A, the survival rate of L929 cells was as low as 40% after exposure to 40 µg/mL of free MINO. By contrast, the cells treated with the equal amount of MINO formulated as Hb-MTN/MINO NPs had

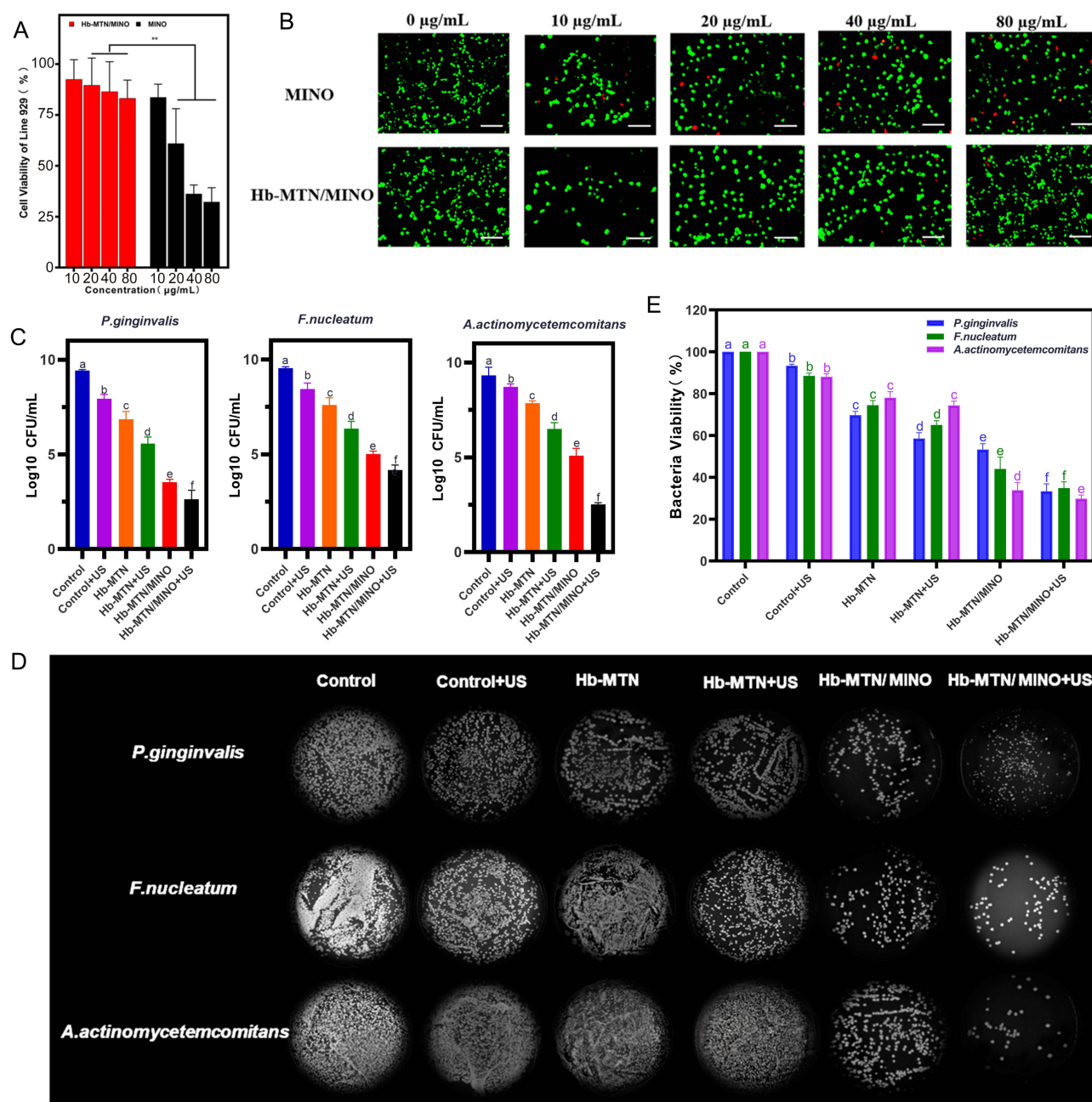


Figure 3 (A) Cytotoxicity of MINO and Hb-MTN/MINO in L929 cells; (B) Live/dead staining images of L929 cells treated with MINO and Hb-MTN/MINO. Antibacterial activities of different treatments against suspended bacteria. (C) CFU counting results. (D) plate image. (E) MTT assessment of the effect on bacterial growth. ** representing $p < 0.01$. Means within columns followed by different letters are significantly different ($p < 0.05$).

a high survival rate of 80%. Although the effect of MINO on the survival of cells was concentration-dependent, L929 cells treated with Hb-MTN/MINO were always significantly more viable than those treated with free MINO. In addition, cells that underwent the same treatment were stained with calcein-AM/EthD and analyzed by confocal fluorescence microscopy (Figure 3B). Consistently, there were a significantly smaller number of cells stained red in the Hb-MTN/MINO group, indicating that more cells survived compared to the treatment with free MINO. Hence, it is reasonable to infer that the potential toxicity of antibiotics can be diminished with the assistance of nanoparticles serving as drug carriers. It stands to reason that the encapsulation of the drug inside the nanoparticles and the slow release are the main reasons for the reduced toxicity. Therefore, we can infer that the cytotoxicity of the antibacterial drug MINO was

significantly reduced when it was loaded into the Hb-MTN nanoparticles, so that the final preparation exhibited a good safety profile with cultured cells, as expected.

Antibacterial Effects of Hb-MTN/MINO NPs

Based on the interaction between ultrasound and nanoparticle-based antibiotic drug delivery systems, the platform was expected to exhibit great antibacterial ability. To further assess the antibacterial properties of Hb-MTN/MINO combined with ultrasonication, three of the most common gingival pathogens (*P. gingivalis*, *F. nucleatum* and *A. actinomycetemcomitans*) were used as model organisms. *P. gingivalis* is considered the major pathogen responsible for chronic periodontitis and is commonly used in animal models, whereas *F. nucleatum* and *A. actinomycetemcomitans* are usually considered to be associated with aggressive periodontitis.³⁴ The continuous growth of microorganisms with the concomitant release of toxins, enzymes and metabolites can stimulate the body's immune response and lead to disease.³⁵ While aSDT deeply penetrates tissues, it selectively kills disease-causing microorganisms with minimal damage to neighboring healthy cells, which makes it a suitable choice for clinical applications.³⁶

First, the bacterial growth curves were recorded in preliminary experiments (Figure S3). Compared with *P. gingivalis* and *A. actinomycetemcomitans*, the growth of *F. nucleatum* was relatively slow. To determine the appropriate antimicrobial concentration, a pre-experiment was performed using Hb-MTN (without MINO loading) to examine its antimicrobial activity. The minimal inhibitory concentration (MIC) was determined based on the absorbance value, as the solution was turbid due to the materials themselves. As shown in Figure S4, a significant difference between the standard lines indicated reduced growth of the bacterial strain at this concentration, confirming intrinsic antibacterial activity. Overall, although a small difference existed among the three microorganisms, the appropriate antimicrobial concentration was 200 µg/mL, which was expected to achieve satisfactory results and avoid side effects as much as possible. Based on these results, the antibacterial performance was evaluated. Additionally, the drug release behavior was assessed over 48 h. The antibacterial effects on the suspended bacteria were evaluated by counting the colony forming units (CFU), as shown in Figure 3C. Without MINO, MTN had limited bactericidal activity. However, the bactericidal effect significantly improved once MINO was encapsulated to form Hb-MTN/MINO nanoparticles. Following treatment with ultrasound-activated Hb-MTN/MINO, the bacterial counts decreased by approximately 3 log compared to the Hb-MTN group. Compared with the control group, the bacterial counts in the ultrasound-activated Hb-MTN/MINO group all decreased by approximately 6 log. Images of the culture plates are shown in Figure 3D. These findings were in agreement with a recent study by Ji et al, who showed that the bacterial count of *P. gingivalis* was reduced by 4.7 log following adjuvant sonodynamic therapy using 40 µg/mL of hematoporphyrin monomethyl ether (HMME).³⁷ These results suggest that ultrasonication activates ROS, playing an essential role in the dynamic treatment modality. When sonosensitizers are exposed to low-intensity focused ultrasound (LIFU), they initiate acoustic cavitation and subsequent generation of ROS.³⁸ These factors can disrupt the structural integrity of the bacterial cell membrane, leading to lysis.³⁹

Moreover, the effects of the material and ultrasonication on metabolic activity were investigated using the MTT assay. As shown in Figure 3E, a trend similar to that of the CFU counts was observed. Both ultrasound and the material itself induce damage to bacterial metabolism, whereby the Hb-MTN/MINO-mediated SDT had a synergistic effect with improved antibacterial activity. Thus, both ultrasonication and the drug system were effective against the periodontal bacteria. In addition to the loaded MINO, when the material of the MTN was stimulated by ultrasonication, the generated ROS contributed to the enhanced antibacterial performance. Therefore, the novel antibiotic-nanoparticle system combined with SDT exhibited improved antibacterial performance and low toxicity, suggesting its potential for therapeutic applications for the treatment of periodontal inflammation and other deep bacterial infections.

In vivo Therapeutic Efficacy of Hb-MTN/MINO NPs Combined with SDT for the Treatment of Periodontal Inflammation in Rat Models

Although satisfactory results were obtained in terms of cell toxicity and antibacterial performance in vitro, further experiments were needed to evaluate the therapeutic efficacy in vivo, taking complicated dental structures into consideration. Based on previous studies, Wistar rat models with periodontal inflammation were established using silk

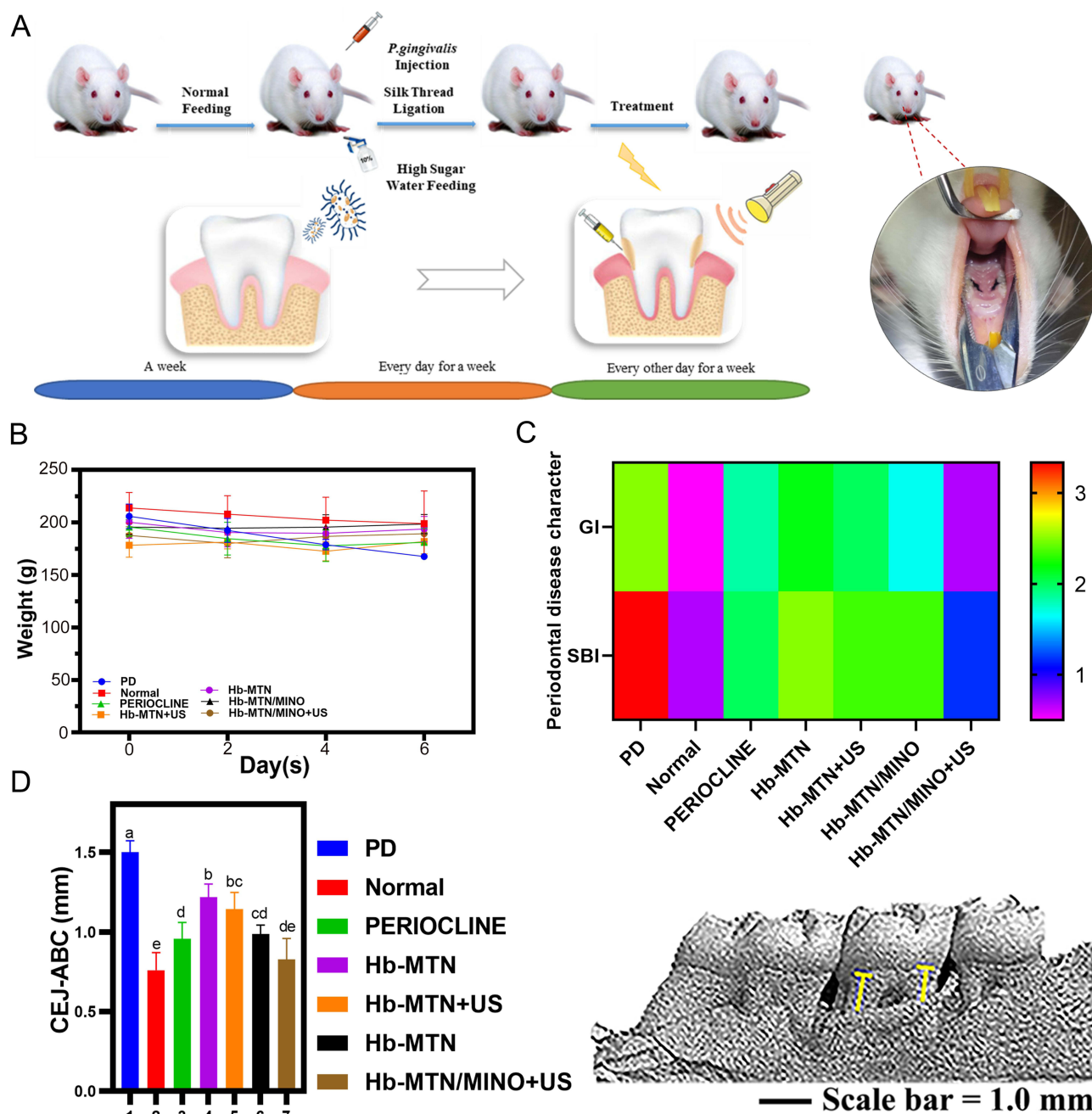


Figure 4 (A) Periodontitis modeling procedure of the second maxillary molar in rats. (B) Weight changes of rats during experimental therapy. (C) Examination of oral condition (GI and SBI). (D) The distance of CEJ-ABC and 3D reconstruction of micro-CT images. Means within columns followed by different letters are significantly different ($p < 0.05$).

ligature and local *P. gingivalis* injection, after which 10% syrup was fed to accelerate the development of periodontitis. After continuous induction, the rat models were successfully established as shown in Figure 4A. The periodontitis model rats were treated as indicated, while a group of healthy rats mock-treated with PBS was included to control for the stimulating effects caused by a local injection. The hemolysis assay is a basic *in vitro* test to determine the safety of blood-contacting nanomaterials.⁴⁰ To ensure treatment safety, a hemolytic assessment of Hb-MTN/MINO was conducted prior to treatment. As shown in Figure S5, the hemolysis rate of erythrocytes treated with Hb-MTN/MINO was concentration-dependent, but was still less than 5%, which indicates that the test material is nonhemolytic and can be used for *in vivo* therapy according to the ASTM E2524-08 standard.⁴¹ During administration, the weight changes of the

rats were recorded as shown in [Figure 4B](#). There was a slight weight decrease even in the healthy group with locally injected PBS, which was caused by stimulation from a local injection in the oral cavity. However, the body weight of the rats began to stabilize or even improved following adaption to the experimental conditions. It was inferred that a local injection in periodontal tissues changed the oral status, but the effect was negligible in the long run. By contrast, rats in the PD group without any treatment experienced continued weight loss, illustrating how periodontal inflammation affects feeding and physical health. After the administration of the therapy, the oral conditions were examined according to clinical standards.

As shown in [Figure 4C](#), rats in the PD group had reddened gums that bled on probing, whereas those in the normal group showed the lowest gingival index (GI) and sulcus bleeding index (SBI). GI and SBI are commonly used to determine periodontal health.⁴² GI is defined as a gingival condition observed by a blunt-headed periodontal probe combined with visual inspection. SBI is defined as the bleeding of the gingival sulcus following pressure from a blunt-headed periodontal probe. Lower scores indicated better gingival health and reduced gingival sulcus bleeding.^{43,44} Therefore, although an equal amount of PBS was injected into healthy rats, stimulating the oral cavity in this way did not significantly affect the health of the periodontal tissues. Compared to the PD group, GI and SBI were reduced in the other treatment groups. Especially in the group treated with Hb-MTN/MINO and ultrasonication, there was only light bleeding on probing, while the GI and SBI scores were close to those of the normal group. Moreover, the scores were significantly better than those of the PERIOCLINE (positive control) group, indicating that the nanodrug delivery system for SDT could alleviate the inflammatory response of the periodontium in rats. Tissue damage is an important indicator of the health of periodontal tissue. The maxillary bone of the rats was scanned and analyzed using a high-resolution micro-CT imaging system, whereby the selected region of interest (ROI) contained the alveolar bone of the second molar near the crown. The parameters related to bone microstructure were analyzed as shown in [Figure S6](#), including BV/TV, Tb.Th, Tb.Sp, and Tb.N. Compared to the PD group, the levels of BV/TV, Tb.Th, and Tb.N increased to varying degrees, while Tb.Sp decreased, providing direct evidence of improved bone structure. In addition, the amount of alveolar bone loss (ABL) was determined by measuring the linear distance from the cemento-enamel junction (CEJ) to the alveolar bone crest (ABC) in the second molar using software to reconstruct 3D images. The ABC-CEJ values were significantly reduced in each treatment group ([Figure 4D](#)). Notably, rats treated with PERIOCLINE and Hb-MTN/MINO combined with ultrasonication showed similar results to healthy rats in the normal group. Therefore, Hb-MTN/MINO-mediated SDT effectively alleviated alveolar bone resorption.

Furthermore, H&E staining was conducted on the second maxillary molar to assess periodontal tissue injury. As shown in [Figure 5A](#), the gingival epithelium was necrotic and loosely bound to the tooth surface in the PD model. By contrast, the gingival epithelium was intact and tightly bound to the surrounding tooth surface in the normal group, with neatly arranged subepithelial connective tissue. Rats with periodontal inflammation showed a slight reduction of symptoms after treatment with Hb-MTN, Hb-MTN with ultrasonication, or Hb-MTN/MINO. In contrast to healthy rats, the gingival epithelium was still partially necrotic. However, Hb-MTN/MINO with ultrasonication led to significant recovery of the damage to the epithelium, with a tighter attachment, similar to the PERIOCLINE group. Although there was still a small amount of lymphocytic infiltration and vascular congestion clearly visible on TEM due to the short period of treatment, the tissue damage was significantly reduced. It stands to reason that the treatment time and frequency of administration could be further extended for a better healing result, but this was beyond the scope of this study. In addition, the serum levels of the inflammatory factors IL-6 and MMP-9 were statistically lower than in the PD group ([Figure S7](#)), indicating that Hb-MTN/MINO with SDT was able to significantly alleviate the inflammation. This finding is similar to the results of Bahrami et al, who showed a significant reduction of IL-6 gene expression following ROS-based antimicrobial therapy using ZnONPs as photo-sonosensitizers in aPDT, aSDT, and antimicrobial photo-sonodynamic therapy (aPSDT).⁴⁵ Although the IL-1 β and TNF- α levels did not change significantly, this may be related to the model construction method and stimulation time. Thus, it can be concluded that these therapies resulted in a certain difference in the expression of inflammatory factors, but relevant mechanisms require more in-depth studies in the future. Furthermore, the blood biochemical parameters were evaluated after treatment, as shown in [Figure 5B](#). Parameters including alanine aminotransferase (ALT), aspartate aminotransferase (AST), total protein (TP), alkaline phosphatase (AKP), blood urea nitrogen (BUN), albumin (ALB) and creatinine (CRE) were improved compared to the periodontitis model group. H&E staining

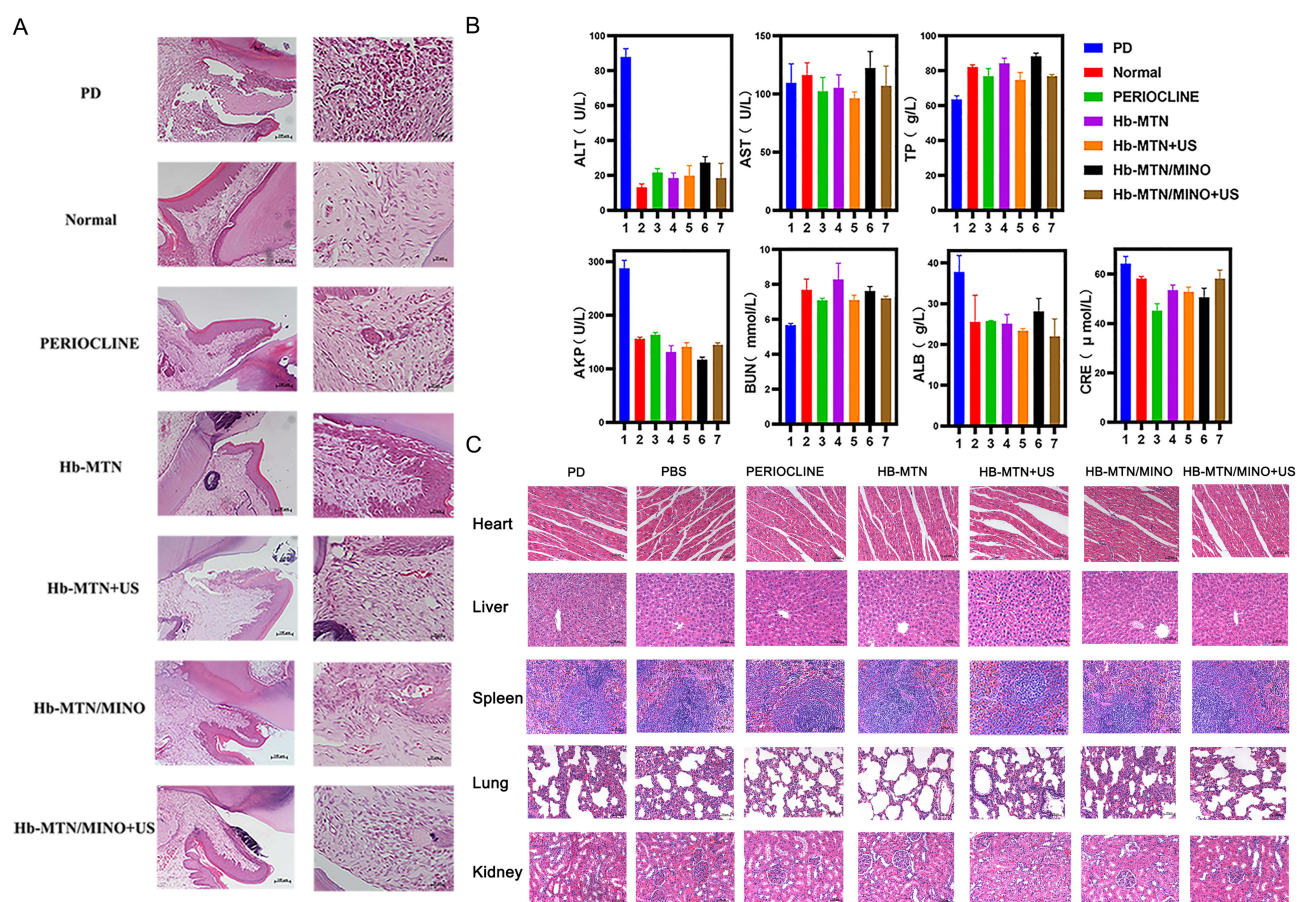


Figure 5 (A) H&E staining of periodontal tissues of second molars in rats. **(B)** Blood biochemical markers (ALT, AST, TP, AKP, BUN, ALB, CRE) of rats after treatment. **(C)** H&E staining images of major organs after treatment.

of the main organs (heart, liver, spleen, lung, and kidneys) also did not reveal significant abnormalities (Figure 5C). These results indicate that the therapeutic modality developed in this study has favorable biosafety with no significant side effects in rats.

In summary, Hb-MTN/MINO-mediated SDT has satisfactory efficacy for the *in vivo* treatment of periodontal inflammation in rats, demonstrating excellent therapeutic potential. Compared with traditional treatments, this method is characterized by better therapeutic efficacy, fewer side effects and less tissue damage. This study therefore provides a reference for further preclinical work on the treatment of periodontitis.

At the same time, it is necessary to recognize the limitations of the current study. Although the nanomaterials have been shown to reduce the bacterial counts of oral pathogens while also demonstrating favorable therapeutic efficacy in a rat model of periodontitis, the clinical application of this antimicrobial treatment and its impact on patient outcomes remains uncertain. Further studies are needed before considering the potential for clinical translation.

Conclusions

In summary, a feasible ultrasound-induced nanoparticle-antibiotic platform was developed in the present study. Based on mesoporous titanium dioxide nanoparticles, this system can be triggered with ultrasound to generate ROS, which already have a bactericidal effect. When combined with loaded antibiotics, a dual antibacterial effects of sonodynamic therapy and chemotherapy is achieved. When combined with SDT, this novel antibiotic-nanoparticle system exhibited improved antimicrobial properties, while achieving lower cytotoxicity compared to conventional therapies. Moreover, it significantly reduced the serum levels of IL-6 and MMP-9. Hb modification on the surface of nanoparticles alleviated hypoxia in periodontal pockets, contributing to ultrasonic activation of ROS generation from O₂. Due to its deep penetration, SDT

potentiates the antibacterial properties of the co-assembled material in periodontal pockets. Therefore, the combination of Hb-MTN/MINO NPs with SDT decreased the limitations of single therapy, providing a new strategy for the treatment of local bacterial periodontitis.

Acknowledgments

This study was supported by the Natural Science Foundation Program of Fujian Province of China (No. 2022J01012).

Disclosure

The authors declare that they have no competing interests in this work.

References

1. Slots J. Periodontitis: facts, fallacies and the future. *Periodontology*. 2017;75(1):7. doi:10.1111/prd.12221
2. Asadi A, Abdi M, Kouhsari E, et al. Minocycline, focus on mechanisms of resistance, antibacterial activity, and clinical effectiveness: back to the future. *J Global Antimicrob Resist*. 2020;22:161–174. doi:10.1016/j.jgar.2020.01.022
3. Bettany JT, Wolowacz RG. Tetracycline derivatives induce apoptosis selectively in cultured monocytes and macrophages but not in mesenchymal cells. *Adv Dent Res*. 1998;12(1):136–143. doi:10.1177/08959374980120010901
4. Whitmore SE, Lamont RJ, Goldman WE. Oral Bacteria and Cancer. *PLoS Pathogens*. 2014;10(3):e1003933. doi:10.1371/journal.ppat.1003933
5. Lundberg K, Wegner N, Yucel-Lindberg T, et al. Periodontitis in RA—the citrullinated enolase connection. *Nat Rev Rheumatol*. 2010;6(12):727. doi:10.1038/nrrheum.2010.139
6. Kebschull M, Papapanou PN. The use of gene arrays in deciphering the pathobiology of periodontal diseases. *Humana Press*. 2010. doi:10.1007/978-1-60761-820-1_24
7. Knnen E, Gursoy M, Gursoy UK. Periodontitis: a multifaceted disease of tooth-supporting tissues. *J Clin Med*. 2019;8(8):1135. doi:10.3390/jcm8081135
8. Zhang S, Yu N, Arce RM. Periodontal inflammation: integrating genes and dysbiosis. *Periodontology*. 2020;82(1):129–142. doi:10.1111/prd.12267
9. Hajishengallis G. Periodontitis: from microbial immune subversion to systemic inflammation. *Nat Rev Immunol*. 2015;15(1):30–44. doi:10.1038/nri3785
10. Eke PI, Thornton-Evans GO, Wei L, et al. Periodontitis in US adults: National Health and Nutrition Examination Survey 2009–2014. *J Am Dent Assoc*. 2018;149(7):576. doi:10.1016/j.adaj.2018.04.023
11. Darveau R. Periodontitis: a polymicrobial disruption of host homeostasis. *Nat Rev Microbiol*. 2010;8:481–490. doi:10.1038/nrmicro2337
12. Pihlstrom BL, Michalowicz BS, Johnson NW. Periodontal diseases. *Lancet*. 2005;366(9499):1809–1820. doi:10.1016/S0140-6736(05)67728-8
13. Bergenholz G, Lindhe J. Effect of experimentally induced marginal periodontitis and periodontal scaling on the dental pulp. *J Clin Periodontol*. 1978;5:59–73. doi:10.1111/j.1600-051x.1978.tb01907.x
14. Genco RJ, Evans RT, Ellison SA. Dental research in microbiology with emphasis on periodontal disease. *J Am Dent Assoc*. 1969;78(5):1016–1036. doi:10.14219/jada.archive.1969.0162
15. Munasur SL, Turawa EB, Chikte UME, Musekiwa A. Mechanical debridement with antibiotics in the treatment of chronic periodontitis: effect on systemic biomarker—a systematic review. *Int J Environ Res Public Health*. 2020;17(15):5601. doi:10.3390/ijerph17155601
16. Adriaens PA, Adriaens LM. Effects of nonsurgical periodontal therapy on hard and soft tissues. *Periodontology*. 2004;36(1):121–145. doi:10.1111/j.1600-0757.2004.03676.x
17. Wang HL, Greenwell H. Nonsurgical periodontal therapy. *Periodontology*. 2010;25(1):89–99. doi:10.1034/j.1600-0757.2001.22250107.x
18. Graziani F, Karapetsa D, Alonso B, et al. Nonsurgical and surgical treatment of periodontitis: how many options for one disease? *Periodontology*. 2017;75(1):152–188. doi:10.1111/prd.12201
19. Zhiqing P, Peicheng X, Jingjing Z, et al. Local delivery of minocycline-loaded PEG-PLA nanoparticles for the enhanced treatment of periodontitis in dogs. *Int J Nanomed*. 2014;9:3963–3970. doi:10.2147/IJN.S67521
20. Herrera D, Molina A, Buhlin K, et al. Periodontal diseases and association with atherosclerotic disease. *Periodontology*. 2020;83:66–89. doi:10.1111/prd.12302
21. Rengeng L, Qianyu Z, Yuehong L, et al. Sonodynamic therapy, a treatment developing from photodynamic therapy. *Photodiagn Photodyn Ther*. 2017;19:159–166. doi:10.1016/j.pdpdt.2017.06.003
22. Hiraoka W, Honda H, Feril LB, et al. Comparison between sonodynamic effect and photodynamic effect with photosensitizers on free radical formation and cell killing. *Ultrason Sonochem*. 2006;13(6):535–542. doi:10.1016/j.ultsonch.2005.10.001
23. Roy J, Pandey V, Gupta I, et al. Antibacterial sonodynamic therapy: current status and future perspectives. *ACS Biomater Sci Eng*. 2021;7:5326–5338. doi:10.1021/acsbiomaterials.1c00587
24. Deepagan VG, You DG, Um W, et al. Long-circulating Au-TiO₂ nanocomposite as a sonosensitizer for ROS-mediated eradication of cancer. *Nano Lett*. 2016;acs.nanolett.6b02547. doi:10.1021/acs.nanolett.6b02547
25. Harada Y, Ogawa K, Irie Y, et al. Ultrasound activation of TiO₂ in melanoma tumors. *J Control Release*. 2011;149(2):190–195. doi:10.1016/j.jconrel.2010.10.012
26. Yoo KC, Yoon CH, Kwon DW, et al. Titanium dioxide induces apoptotic cell death through reactive oxygen species-mediated Fas upregulation and Bax activation. *Int J Nanomed*. 2012;7:1203–1214. doi:10.2147/IJN.S28647
27. Qinqin J, Bin Q, Xiaohong L, et al. A hydrogen peroxide economizer for on-demand oxygen production-assisted robust sonodynamic immunotherapy. *Theranostics*. 2022;12(1). doi:10.7150/thno.64862
28. Loesche WE, Gusberti F, Mettraux G, Higgins T, Syed S. Relationship between oxygen tension and subgingival bacterial flora in untreated human periodontal pockets. *Infect Immun*. 1983;42:659–667. doi:10.1128/iai.42.2.659-667.1983

29. Leme AFP, Koo H, Bellato CM, et al. The role of sucrose in cariogenic dental biofilm formation--new insight. *J Dent Res*. 2006;85(10):878. doi:10.1177/154405910608501002
30. Marsh PD. Are dental diseases examples of ecological catastrophes? *Microbiology*. 2003;149(2):279–294. doi:10.1099/mic.0.26082-0
31. Koo H, Xiao J, Klein MI, et al. Exopolysaccharides produced by streptococcus mutans glucosyltransferases modulate the establishment of microcolonies within multispecies biofilms. *J Bacteriol*. 2010;192(12):3024–3032. doi:10.1128/JB.01649-09
32. Sies H, Jones DP. Reactive oxygen species (ROS) as pleiotropic physiological signalling agents. *Nat Rev mol Cell Biol*. 2020;21(7):363–383. doi:10.1038/s41580-020-0230-3
33. Borisov VB, Siletsky SA, Nastasi MR, et al. ROS defense systems and terminal oxidases in bacteria. *Antioxidants*. 2021;10(6):839. doi:10.3390/antiox10060839
34. Ebbers M, Lübcke PM, Volzke J, et al. Interplay between *P. gingivalis*, *F. nucleatum* and *A. actinomycetemcomitans* in murine alveolar bone loss, arthritis onset and progression. *Sci Rep*. 2018;8. doi:10.1038/s41598-018-33129-z
35. Ebersole JL, Taubman MA, Smith DJ, et al. Human immune responses to oral micro-organisms. I. Association of localized juvenile periodontitis (LJP) with serum antibody responses to *Actinobacillus actinomycetemcomitans*. *Clin Exp Immunol*. 1982;47(1):43–52.
36. Pourhajibagher M, Bahador A. Attenuation of *Aggregatibacter actinomycetemcomitans* virulence using curcumin-decorated nanophytosomes-mediated photo-sonoantimicrobial chemotherapy. *Sci Rep*. 2021;11(1). doi:10.1038/s41598-021-85437-6
37. Ji Z, Zhang H, Zhuang D, et al. Sonodynamic therapy as an adjunctive treatment on porphyromonas gingivalis induced periodontitis in rats with diabetes. *bioRxiv*. 2018. doi:10.1101/450585
38. Pourhajibagher M, Bahrami R, Bahador A. Application of antimicrobial sonodynamic therapy as a potential treatment modality in dentistry: a literature review. *J Dent Sci*. 2024;19(2):787–794. doi:10.1016/j.jds.2023.11.006
39. Canavese G, Ancona A, Racca L, et al. Nanoparticle-assisted ultrasound: a special focus on sonodynamic therapy against cancer. *Chem Eng J*. 2018;340:155–172. doi:10.1016/j.cej.2018.01.060
40. Ilinskaya AN, Dobrovolskaia MA. Nanoparticles and the blood coagulation system. Part II: safety concerns. *Nanomedicine*. 2013;8(6):969–981. doi:10.2217/nnm.13.49
41. Standard test method for analysis of hemolytic properties of nanoparticles. E56.03. 2022.
42. Shen X, Yu Z. The effects of bracketless invisible orthodontics on the PLI, SBI, SPD, and GI and on the satisfaction levels in children with malocclusions. *Am J Transl Res*. 2021;13(5):5066–5072.
43. Chiu S, Lee Y, Liu M, et al. Evaluation of the marginal adaptation and gingival status of full-crown restorations using an intraoral camera. *BMC Oral Health*. 2022;22. doi:10.1186/s12903-022-02587-3
44. Newbrun E. Indices to measure gingival bleeding. *J Periodontol*. 2017;67(6). doi:10.1902/jop.1996.67.6.555
45. Rashin B, Maryam P, Steven P, et al. Anti-biofilm and bystander effects of antimicrobial photo-sonodynamic therapy against polymicrobial periopathogenic biofilms formed on coated orthodontic mini-screws with zinc oxide nanoparticles. *Photodiagnosis Photodyn Ther*. 2023;41. doi:10.1016/j.pdpdt.2023.103288

International Journal of Nanomedicine

Publish your work in this journal

The International Journal of Nanomedicine is an international, peer-reviewed journal focusing on the application of nanotechnology in diagnostics, therapeutics, and drug delivery systems throughout the biomedical field. This journal is indexed on PubMed Central, MedLine, CAS, SciSearch®, Current Contents®/Clinical Medicine, Journal Citation Reports/Science Edition, EMBase, Scopus and the Elsevier Bibliographic databases. The manuscript management system is completely online and includes a very quick and fair peer-review system, which is all easy to use. Visit <http://www.dovepress.com/testimonials.php> to read real quotes from published authors.

Submit your manuscript here: <https://www.dovepress.com/international-journal-of-nanomedicine-journal>

Dovepress
Taylor & Francis Group